Chapter 10
Analysis of Debond Fracture Specimens

Several test methods for determining the fracture toughness of the face/core interface in sandwich specimens have been proposed. All debond specimens are beam specimens where a debond typically is implanted in the form of a thin Teflon sheet between face and core during manufacture of the sandwich panel, or in some cases the debond is machined or cut with a thin blade or knife. This and several other experimental issues will be discussed in Chapter 11. In this chapter, we will introduce some of the most popular sandwich debond tests and outline analysis of compliance and energy release rate.

10.1 Introduction

The analysis of the fracture test specimens typically focuses on the global specimen compliance, C. Once this quantity is determined as a function of crack length, the energy release rate G is readily obtained by differentiation of C with respect to crack length a (see Chapter 9), i.e.,

$$G = \frac{P^2}{2b}\frac{dC}{da}, \tag{10.1}$$

where P is the load applied and b is the width of the specimen. Several of the fracture specimens in use are quite simple in terms of geometry, loading, and support conditions, allowing for analytical solution of the compliance as a function of crack length, i.e., $C = C(a)$. Differentiation according to Equation (10.1) yields G. Some fracture specimens, however, are more complicated and do not readily allow an analytical solution. For such specimens, it may be possible to experimentally determine the compliance at several crack lengths. The data could be graphed vs. crack length and an empirical

L.A. Carlsson and G.A. Kardomateas, *Structural and Failure Mechanics of Sandwich Composites*, Solid Mechanics and its Applications 121, DOI 10.1007/978-1-4020-3225-7_10,

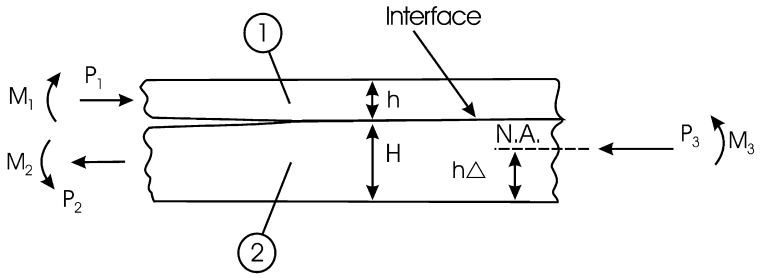

Figure 10.1 Section of cracked bimaterial specimen with an interface crack. Axial forces and moments are applied along the three edges (after Suo and Hutchinson, 1990). The product $h\Delta$ is the distance between the neutral axis and the bottom surface. h is the thickness of the upper beam.

equation, $C = C(a)$ may be obtained by curve-fitting. Ideally, the form of the compliance expression, $C = C(a)$, is known from experience or analysis. Differentiation of $C(a)$ with respect to crack length according to Equation (10.1) yields G. This approach, however, may not work well for tests where the compliance changes very little with crack length, or where the form of $C = C(a)$ is not guided by analysis.

As an alternative to a complete solution for the compliance of a fracture specimen Yin and Wang (1984) proposed consideration of a cut-out section from a cracked laminate where axial loads and moments are applied on the edges of the cut-out sections. They developed an analytical procedure to calculate G for a cracked monolithic composite based on the J integral This method was modified and later extended to bimaterial specimens with an interface crack by Suo and Hutchinson (1990) (see Figure 10.1).

However, a sandwich specimen is not homogeneous or bimaterial. A sandwich specimen could be considered as a trimaterial with two faces that can be different and a core. For this case the analysis presented in Section 9.4 should apply (see also Kardomateas et al., 2010).

Most sandwich test specimens are loaded by transverse shear forces. Until recently such loads have not been considered in crack element formulations. Li et al. (2004) and Thouless (2009) developed a finite element approach where transverse shear forces acting on the cracked element are included (see Figure 10.2). Li et al. (2004) found that shear loading causes "root rotation" of the crack tip. Through extensive finite element computations, they found that such rotations affect not only the energy release rate but also the mode mixity, as quantified by the phase angle ψ

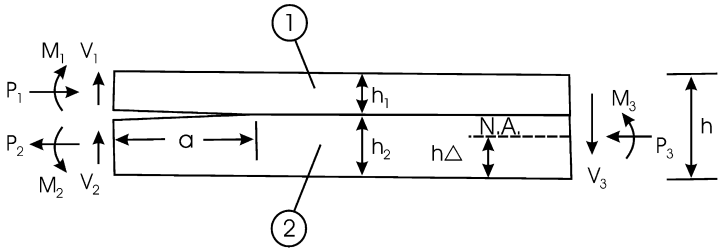

Figure 10.2 Bending moment, axial loads and transverse shear forces acting on segments of a cracked beam geometry. (After Thouless, 2009)

$$\psi = \tan^{-1}\left(\frac{K_{\mathrm{II}}}{K_{\mathrm{I}}}\right), \tag{10.2}$$

where K_{I} and K_{II} are the mode I and mode II stress intensity factors (assuming $\beta = 0$) defined in Chapter 9. The shear effect is greatest for specimens with short crack lengths (compared to the thickness). For long crack lengths, the shear contribution becomes negligible and the previous methods based on axial forces and edge moments only should be valid.

The cracked element approach has many merits. Provided the basic loading parameters, axial load, moment, and transverse shear force are identified, general solutions to difficult problems can be obtained, see a recent paper by Thouless (2009).

10.2 Debond Test Specimens

Several debond sandwich test specimens have emerged. A successful debond test should promote the desired face/core debond propagation failure before any competing failure mode, such as core shear, core crush, indentation failure, face wrinkling, or crack kinking, occurs. Commonly, the test specimens have to be properly designed in order to promote debond growth, and guidelines will be provided in this chapter.

Figure 10.3 shows some of the more widely used debond test specimens for sandwich constructions, viz., the double cantilever beams (DCB), tilted sandwich debond (TSD), cracked sandwich beam (CSB), three-point sandwich beam (TPSB), mixed mode bending (MMB), and DCB-uneven bending moment (DCB-UBM) specimens, each of uniform width (b) and loaded in bending. The specimens shown in Figures 10.3a–d are so-called "fixed mode ratio specimens", since the mode ratio is fixed by the material combi-

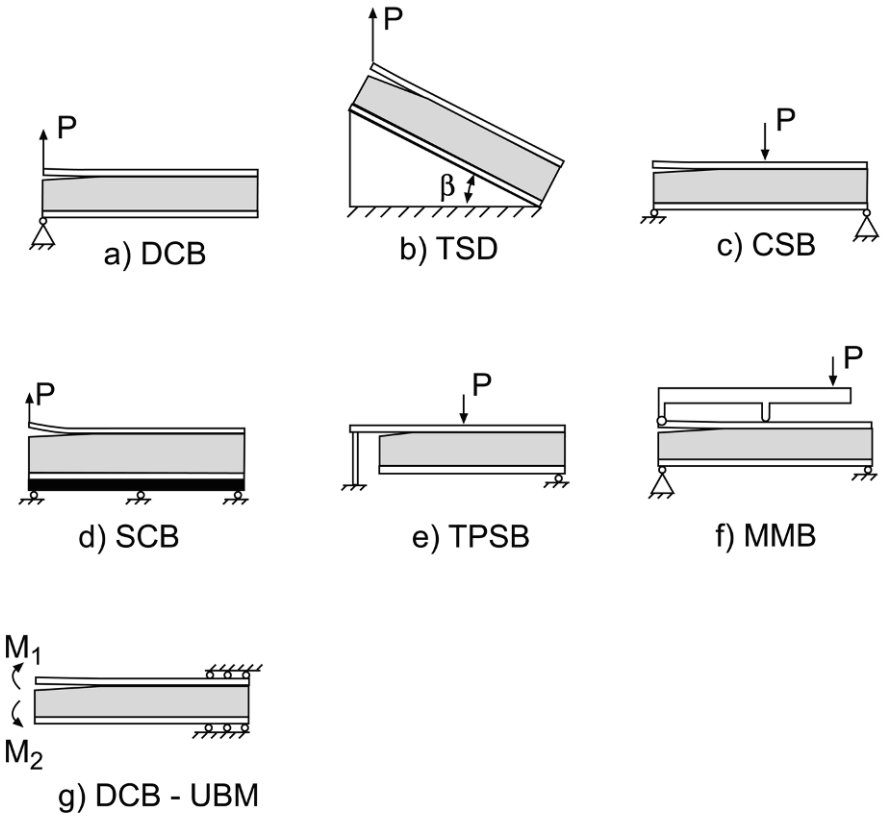

Figure 10.3 Debond sandwich test specimens. (a) DCB, (b) TSD, (c) CSB, (d) SCB, (e) TPSB, (f) MMB, and (g) DCB-UBM.

nation, loading configuration, and specimen geometry, while the specimens in Figures 10.3e and f allow adjustment of the mode mixing. Each of these specimens will be described and available expressions for the compliance and energy release rate will be provided.

10.3 Double Cantilever Beam (DCB) Specimen

The double cantilever beam (DCB) specimen is a very popular test for determining the mode I delamination resistance of laminated composites, and is standardized by ASTM (ASTM D5528, 2001). In DCB testing of composites, the initial delamination is placed symmetrically at the mid-plane. For

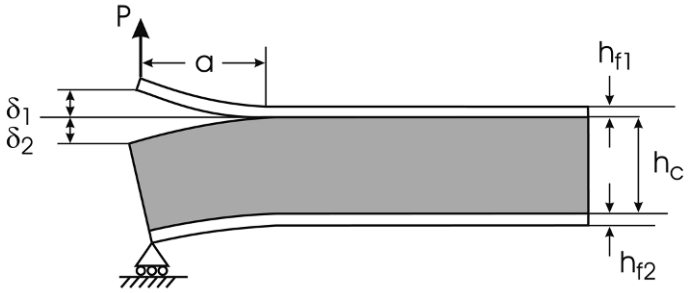

Figure 10.4 Geometry and loading of the sandwich DCB specimen.

the sandwich DCB test, the initial precrack is placed between the upper face sheet and the core to promote face/core debonding (see Figure 10.4). The sandwich DCB specimen was first adopted by Prasad and Carlsson (1994) who conducted testing and finite element analysis of the specimen. They showed that the sandwich DCB specimen is not a pure mode I test as a result of the off-centered crack at a bimaterial interface between widely dissimilar materials. In many cases, experimental testing revealed that crack propagation did not occur at the face/core interface. The crack kinked into the core, as will be discussed later in this section. Shivakumar et al. (2004), however, successfully achieved face/core debond fracture in experimental studies using the sandwich DCB specimen and this will be further discussed in Chapter 11.

In this section, elastic foundation analysis of the compliance and energy release rate of the sandwich DCB specimen will be reviewed. The upper leg of the DCB specimen, i.e. the debonded face sheet (Figure 10.4) is considered as a cantilever beam of effective flexural modulus E_{f1} and thickness, h_{f_1}. The lower leg consists of the lower face, of modulus E_{f2}, and thickness h_{f2}, bonded to a core of modulus, E_c, and thickness h_c. Under load, the loading point (1) displaces an amount $\delta_1 + \delta_2$, where the individual displacements δ_1 and δ_2 are defined in Figure 10.4.

Figure 10.5 illustrates the elastic foundation model (EFM) of the DCB specimen developed by Aviles and Carlsson (2007a). The bonded part of the upper face sheet is supported by the core represented by an elastic foundation. The total specimen length is L and a is the crack length. The elastic foundation is characterized by the foundation modulus k.

The analysis is based on the Winkler foundation model, first applied to isotropic and symmetric DCB specimens by Kaninnen (1973). The Winkler model assumes that the reaction forces in the elastic foundation are propor-

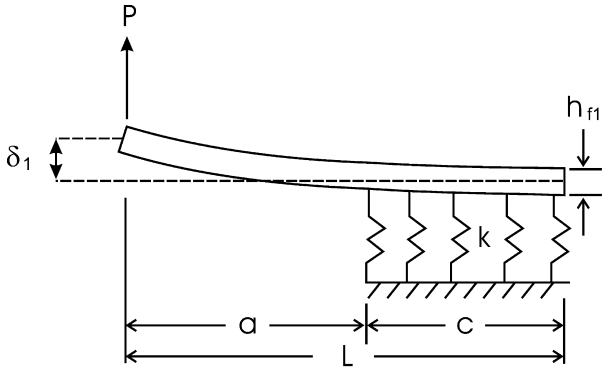

Figure 10.5 Schematic of elastic foundation model (EFM) of a sandwich DCB specimen.

tional to the beam deflection at any point. The foundation modulus, k, is defined as the force required to displace a unit area of the face through a unit distance in the thickness direction. k may be related to the extensional out-of-plane stiffness of the core (Allen, 1969; Kanninen, 1973; see also Chapter 8),

$$k = \frac{2E_c b}{h_c}, \tag{10.3}$$

where b is the width of the specimen. Quispitupa et al. (2009), however, argued that this equation in effect assumes that one half of the core is active as a foundation which is not realistic for thick cores. Quispitupa et al. (2009) proposed the following modified elastic foundation modulus for a sandwich DCB specimen

$$k = \frac{2E_c b}{h_{f1}}. \tag{10.4}$$

Expressions for compliance and energy release rate of a symmetric DCB sandwich specimen were derived by Aviles and Carlsson (2007a),

$$C = \frac{a}{b}\left[\frac{1}{h_c G_{xz}} + \frac{a^2}{3\left(D - \frac{B^2}{A}\right)}\right] + \frac{4}{E_{f1} h_{f1}^3 b}\left[a^3 + 3a^2\eta^{1/4} + 3a\eta^{1/2} + \frac{3}{2}\eta^{3/4}\right], \tag{10.5}$$

$$G = \frac{P^2}{2b^2}\left[\frac{1}{h_c G_{xz}} + \frac{a^2}{\left(D - \frac{B^2}{A}\right)} + \frac{12}{E_{f1}h_{f1}^3}\left[a^2 + 2a\eta^{1/4} + \eta^{1/2}\right]\right], \tag{10.6}$$

$$\eta = \frac{h_{f1}^3 b E_{f1}}{3k}, \tag{10.7}$$

where P is the applied load and the A, B and D terms are the extensional, coupling and bending stiffnesses defined for a general laminated beam in Equations (9.27). For the lower leg of the DCB specimen (lower face bonded to the core)

$$A = E_{f2}h_{f2} + E_c h_c, \tag{10.8a}$$

$$B = h_{f2}h_c\frac{E_c - E_{f2}}{2}, \tag{10.8b}$$

$$D = \frac{1}{12}\left[E_{f2}\left(h_{f2}^3 + 3h_{f2}h_c^2\right) + E_c\left(h_c^3 + 3h_{f2}^2 h_c\right)\right]. \tag{10.8c}$$

To illustrate the foundation effect on the DCB specimen compliance, we will consider a specific (baseline) sandwich DCB specimen. The specimen was obtained from a symmetric sandwich consisting of 2.41 mm thick glass/vinylester face sheets over a 37.9 mm thick H100 PVC foam core. The core is assumed to be isotropic with mechanical properties $E_c = 105$ MPa, $\nu_c = 0.32$, and $G_{xz} = 39.8$ MPa. The mechanical properties of the face sheets are $E_f = 27.6$ GPa and $\nu_f = 0.32$. The face modulus and Poisson ratio refer to loading along the beam axis. In addition, DCB specimens with a range of core moduli $E_c = 10$–800 MPa and a range of total lengths $L = 5$–50 cm were considered. The core shear modulus, G_{xz}, was calculated from E_c using the isotropic relation between the Young's and shear moduli assuming a constant Poisson ratio $\nu_c = 0.32$. The crack length was fixed ($a = 5$ cm).

Figure 10.6a shows the specimen compliance as a function of core modulus. The compliance depends quite strongly on the core modulus and reaches high values for compliant cores ($E_c < 20$ MPa). Figure 10.6b shows the compliance vs. specimen length. The compliance becomes independent of specimen length above a certain length. When the specimen length decreases and becomes comparable to the crack length, however, the compliance increases sharply due to lack of support of the loaded upper face sheets.

This analysis may be used to determine an upper limit on the crack extension for a given test specimen. Calculations by Aviles and Carlsson (2007a) reveal that end-effects are negligible if the crack length is below

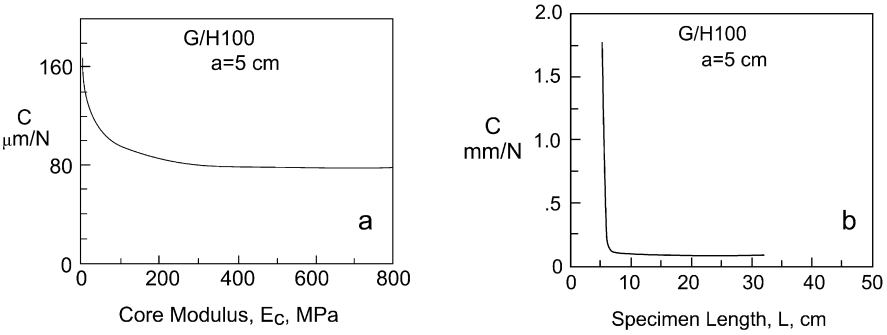

Figure 10.6 DCB specimen compliance. (a) Influence of core modulus, (b) influence of specimen length ($a = 5$ cm).

$$a \leq L - \frac{4.5}{\lambda}, \tag{10.9}$$

where λ is given by

$$\lambda = \sqrt[4]{\frac{3k}{E_{f1} b h_{f1}^3}}. \tag{10.10}$$

For the specific DCB specimen considered here, Equation (10.8) yields $a/L < 0.63$. Hence, to avoid influence of end-effects on the compliance, fracture testing should stop once the crack length, a, reaches 0.63 L.

The accuracy of the analytical model for the DCB compliance was evaluated by Quispitupa et al. (2009), using detailed two-dimensional finite element analysis (FEA). DCB specimens of total length $2L \approx 150$ mm, $b = 35$ mm, $h_{f1} = h_{f2} = 2$ mm and core thicknesses h_c of 10, 20, and 30 mm were analyzed over a range of crack lengths from 5 to 65 mm. The face and core material were E-glass/polyester and H100 PVC foam. The face and core moduli were $E_{f1} = E_{f2} = E_f = 16.4$ GPa, and $E_c = 135$ MPa. The compliance C and energy release rate G were determined from the elastic foundation model, Equations (10.5) and (10.6), and FEA.

Compliance and energy release rate results are shown vs. crack length in Figure 10.7. The energy release rate was calculated using a unit load, $P = 1$ N/mm. Predictions of C and G using the foundation model are in excellent agreement with FEA for the range of face and core materials and geometries considered.

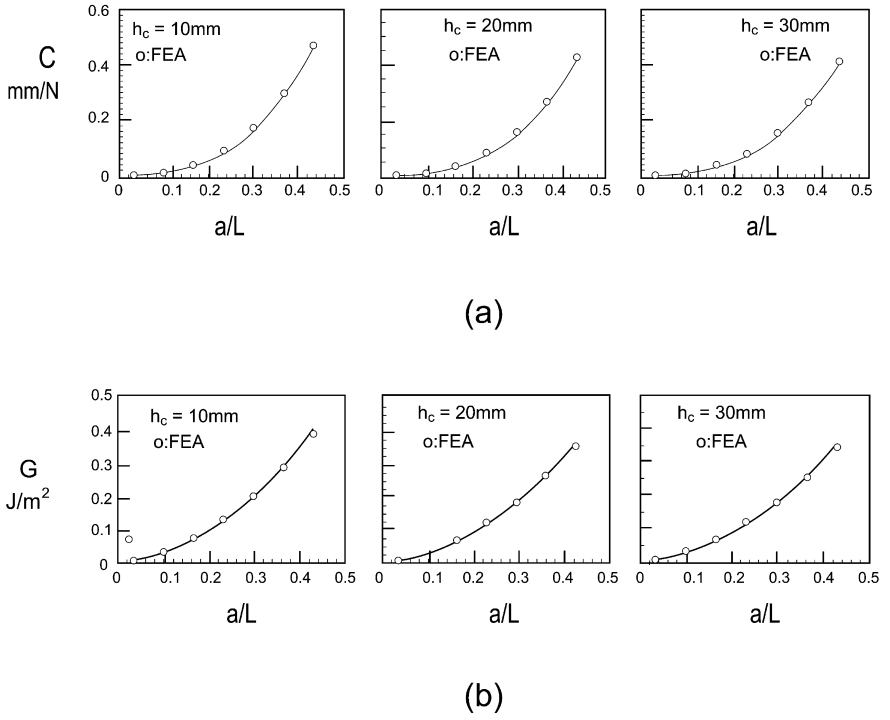

Figure 10.7 Compliance and energy release rate of sandwich DCB specimens. Open circles represent FEA, and the continuous line the elastic foundation model (after Quispitupa et al., 2009). For the calculation of G, a load $P = 1$ N/mm was used.

10.3.1 Crack Kinking Analysis

Crack kinking analysis of a DCB sandwich specimen will be discussed for some specific specimens. Details and assumptions of the crack kinking analysis are outlined in Section 9.2. Two-dimensional, plane strain finite element models of foam cored DCB specimens with aluminum face sheets were constructed to calculate the crack tip stress intensity factors, K_{I} and K_{II} (Prasad and Carlsson, 1994a). The face sheets were 2.2 mm thick and had the following mechanical properties: $E_f = 70$ GPa and $\nu_f = 0.3$. The adhesive layer between face and core was assumed to be 0.1 mm thick, with $E_a = 3.5$ GPa and $\nu_a = 0.35$. The core was 20 mm thick and was considered to have a range of properties from "stiff" to "soft"; $E_c = 9.7 - 0.28$ GPa, and $\nu_c = 0.35$. The crack length was 25.4 mm, and the total specimen length was 152 mm.

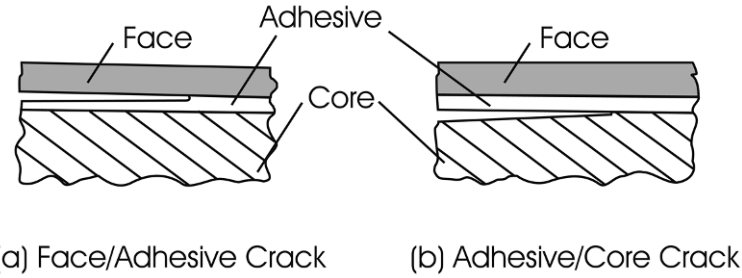

Figure 10.8 Crack configurations examined. (a) Face/adhesive interface crack, (b) adhesive/core interface crack.

The crack may propagate at the face/adhesive or adhesive/core interfaces, or it may kink away from the interface. Hence, the two interface crack configurations illustrated in Figure 10.8 were considered.

It is recognized that both interface configurations involve a crack between two isotropic materials which allows application of Equation (9.9) for determination of the stress intensity factors, K_{I} and K_{II},

$$\delta_{\mathrm{I}} + i\delta_{\mathrm{II}} = 4\sqrt{\frac{x}{2\pi}\left(\frac{1}{\overline{E}_1} + \frac{1}{\overline{E}_2}\right)}(K_{\mathrm{I}} + iK_{\mathrm{II}}). \tag{10.11}$$

Subscripts 1 and 2 denote the material number above and below the crack plane. For the face/adhesive crack configuration, material #1 is aluminum while material #2 is epoxy, and for the adhesive/core configuration, material #1 is epoxy and material #2 is the core. δ_I and δ_{II} are the opening and sliding crack face displacements illustrated in Figure 9.4, and $\overline{E} = E$ for plane stress, and $E/(1-\nu^2)$ for plane strain. Each specimen was loaded by a unit load ($P = 1$ N/mm).

A complete analysis to determine whether or not the crack tip would continue to propagate as an interface crack, or if it would kink, would involve Equation (9.26),

$$\frac{G^K_{\max}}{G} > \frac{G_{IC}}{G_c}, \tag{10.12}$$

where $G^k_{\max}$ is the maximum energy release rate for the kinked crack, G is the energy release rate for the interface crack, G_{IC} the mode I fracture toughness of the core, and G_c the interface fracture toughness.

Hence, characterization of crack kinking requires elaborate analysis and key material toughnesses. It should be pointed out that the determination of the interface toughness, G_c, may not be possible if the interface is tough

and if kinking occurs. In such a case, it is still possible to assess kinking, but in a more qualitative manner by examining the angle, Ω, the interface crack would deflect if it were to kink. A negative kink angle, $\Omega \leq 0$, would indicate interface growth (no kinking) or kinking up into face sheet, which is not physically impossible if the face sheets are tough. On the other hand, a positive angle $\Omega > 0$, indicates the tendency for kinking into the core which is possible for brittle polymer foams.

The kink angle, Ω, of the foam core DCB specimens considered is first calculated from Equation (9.24), derived for a mixed mode crack in a homogeneous, isotropic brittle material. The kink angle was also determined from the rigorous analysis of He and Hutchinson (1989), with kink angles depicted in graphical form in their paper. The He and Hutchinson kinking analysis requires specification of Dundurs' (1969) elastic bimaterial mismatch parameter, α,

$$\alpha = \frac{\overline{E}_1 - \overline{E}_2}{\overline{E}_1 + \overline{E}_2}, \tag{10.13}$$

where $\overline{E}$ is defined under Equation (10.11). The parameter α ranges from -1 to 1, where the limits are approached when one material is much stiffer than the other. If the materials 1 and 2 above and below the crack plane are the same, $\alpha = 0$. For the foam core sandwich DCB specimens considered here, α is close to the upper limit ($\alpha \approx 1$). The analysis of He and Hutchinson (1989) provides the kink angle Ω for material combinations with α within $-0.75 < \alpha < 0.75$. For some of the extreme cases considered here, α falls outside this range. For such cases the results for $\alpha = 0.75$ are used.

Figure 10.9 displays kink angle results for the foam core DCB specimens with face/adhesive and adhesive/core interface cracks over the range of core moduli investigated. For DCB specimens with a stiff core ($E_f/E_c \leq 20$) the kink angle is negative and such specimens are not expected to display kinking down into the core ($\Omega < 0$). Kinking up into the tough aluminum face sheets is highly unlikely. For a DCB specimen with a low modulus core, however, the positive value of Ω indicates that an interface crack may leave the interface and enter into the core at an angle which somewhat depends on the actual crack configuration (Figure 10.8). The kink angle is larger for the face/adhesive interface crack than for the adhesive/core crack. It is furthermore observed in Figure 10.9 that the crack kinking analysis of He and Hutchinson (1989), labeled "bimaterial", consistently predicts a larger kink angle than Equation (9.24), labeled "homogeneous", but the difference is less than 5° for all cases investigated.

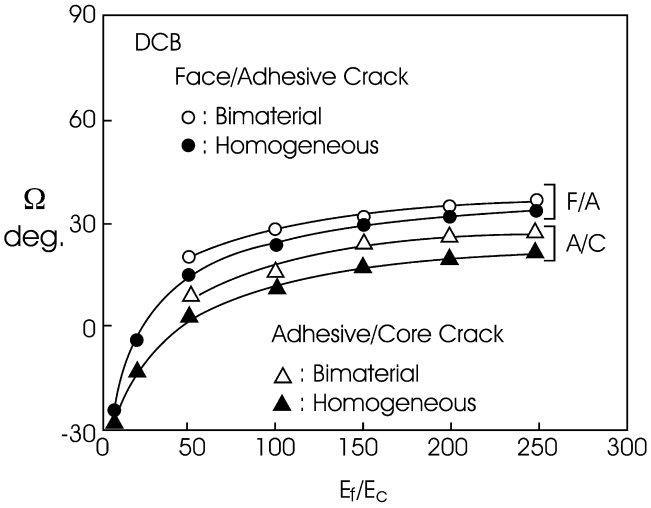

Figure 10.9 Kink angle vs. face/core modulus ratio for DCB sandwich specimens with aluminum face sheets ($a = 25.4$ mm).

10.4 Tilted Sandwich Debond (TSD) Specimen

The tilted sandwich debond (TSD) specimen, shown in Figure 10.10 was introduced as a debond test for foam cored sandwich specimens by Li and Carlsson (1999). The specimen is tilted at an angle, θ, and loaded by a vertical force, P. This force may be resolved into axial and normal components, P_A, and P_N,

$$P_A = P \sin\theta, \tag{10.14a}$$

$$P_N = P \cos\theta. \tag{10.14b}$$

It was initially thought that the TSD specimen would allow mixed mode debond testing. By changing the tilt angle, θ, the mode ratio, e.g. $K_{\mathrm{II}}/K_{\mathrm{I}}$, would also change. As will be discussed, however, this idea is not supported by detailed analysis. Still, testing of foam cored sandwich specimens reveals that this specimen configuration is less prone to crack kinking than the DCB specimen discussed in Section 10.4.

Analysis of the TSD specimen based on elastic foundation modeling has been presented by Li and Carlsson (2000). Figure 10.11 defines several of the geometry symbols, such as the crack length a and the bonded length l. The loaded face sheet (Figure 10.11) is considered a beam on an elastic foundation. The applied load P may be resolved into axial and normal components, Equations (10.14). The analysis is based on superposition of solutions for the

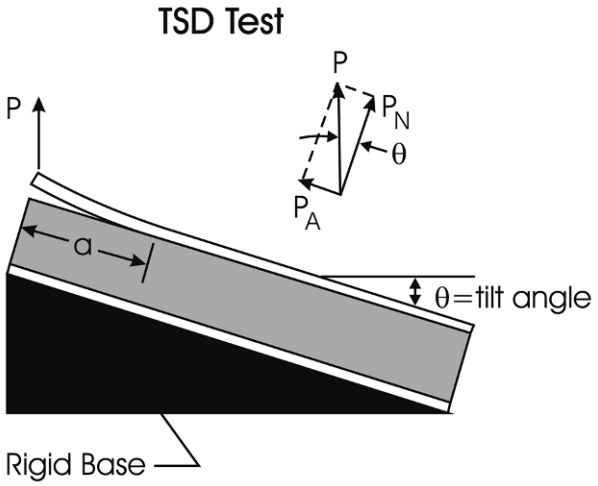

Figure 10.10 TSD specimen. θ is the tilt angle.

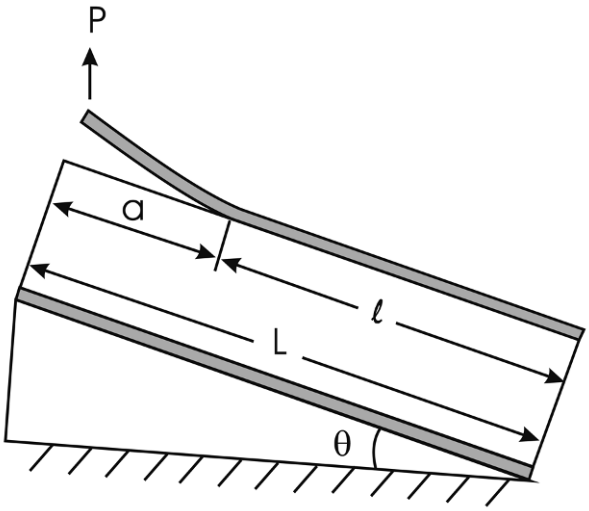

Figure 10.11 TSD specimen loading and geometry.

face sheet being subjected to an edge force and edge moment at the left end of the bonded region (at the crack tip). In addition, the face will deflect due to the normal force component, P_N, and the core will deform in shear due to the axial component, P_A.

Li and Carlsson (2000) used a one-parameter foundation model for the bonded region, with a foundation modulus, k, given by the classical expres-

sion, Equation (10.3), here adjusted for the fact that only one face is loaded in the TSD configuration,

$$k = \frac{E_c b}{h_c}, \tag{10.15}$$

where E_c is the core modulus, b the specimen width, and h_c the core thickness. An expression for the displacement of the upper face sheet was derived (Li and Carlsson, 2000). The bending compliance, defined as the deflection of the loading point perpendicular to the specimen axis, divided by the normal force component, P_N, is given by

$$C_1 = \frac{4\beta}{k}\left\{\frac{1}{3}\beta^3 a^3 + \beta^2 a^2 + \beta a + \frac{1}{2}\right\}, \tag{10.16}$$

where

$$\beta = \left(\frac{k}{4E_f I_f}\right)^{1/4}, \tag{10.17a}$$

$$I_f = \frac{h_f^3}{12} \tag{10.17b}$$

Equation (10.16) is valid only for crack lengths less than a limit crack length, where end-effects start to contribute to the compliance

$$a \leq L - 3\left(\frac{E_f h_f^3 h_c}{3E_c}\right)^{1/4}. \tag{10.18}$$

This explicit equation may be used for determining how long cracks may be used in an experimental test program.

In addition to the normal deflection of the face, the point of load application will displace axially due to the action of the axial force component, P_{II}. This deformation will consist of extension of the face under tension and shear deformation of the core. This contribution is generally small and may be neglected. For such a case, the load point compliance, $C = \delta/P$, where δ is the vertical displacement component, becomes

$$C = \frac{4\beta}{k}\left\{\frac{1}{3}\beta^3 a^3 + \beta^2 a^2 + \beta a + \frac{1}{2}\right\}\cos^2\theta. \tag{10.19}$$

Differentiation of Equation (10.19) with respect to crack length, yields the energy release rate

$$G = \frac{4\beta P^2}{2bk}(\beta a + 1)^2 \cos^2\theta. \tag{10.20}$$

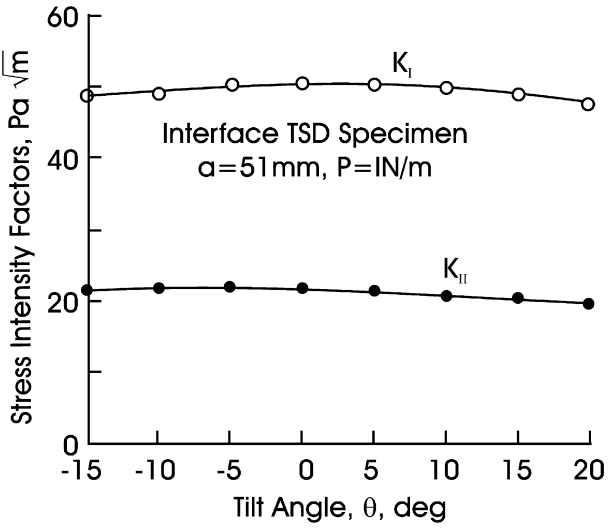

Figure 10.12 Interface stress intensity factors vs. tilt angle for the TSD specimen.

10.4.1 Mode Mixity Analysis

Several TSD configurations were analyzed by Li and Carlsson (2001). We will here reproduce results for the "interface configuration" where a 51 mm long crack is supposed to lie on the interface between a 3.6 mm thick face sheet and a 50 mm thick core. The glass/epoxy face and H100 core moduli were: $E = 21.2$ GPa and $E_c = 99$ MPa. To examine the influence of tilt angle, θ on the interface stress intensity factors, K_{I} and K_{II}, finite element calculations were conducted over a range of tilt angles (–15° to 20°).

Figure 10.12 displays K_{I} and K_{II} vs. tilt angle θ. It is observed that K_{I} and K_{II} remain essentially independent of the tilt angle. Because $K_{\mathrm{II}} > 0$, for the tilt angles considered, the face/core crack would have a tendency to kink down into the core ($\Omega > 0$) and would do so unless the interface is weak and the core is tough.

Further analysis of the stress intensity factors was conducted for a TSD specimen at zero tilt angle over a range of core stiffnesses. In this analysis, the face sheet thickness and modulus were kept as above while the core modulus was varied. The kink angle, Ω, was calculated from Equation (9.24) based on the stress intensity factors K_{I} and K_{II}. Figure 10.13 shows the kink angle plotted vs. the face-to-core modulus ratio, E_f/E_c. For modulus ratios greater than about 20, the kink angle changes sign from negative to positive. Above this modulus ratio, crack kinking into the core is a possibility.

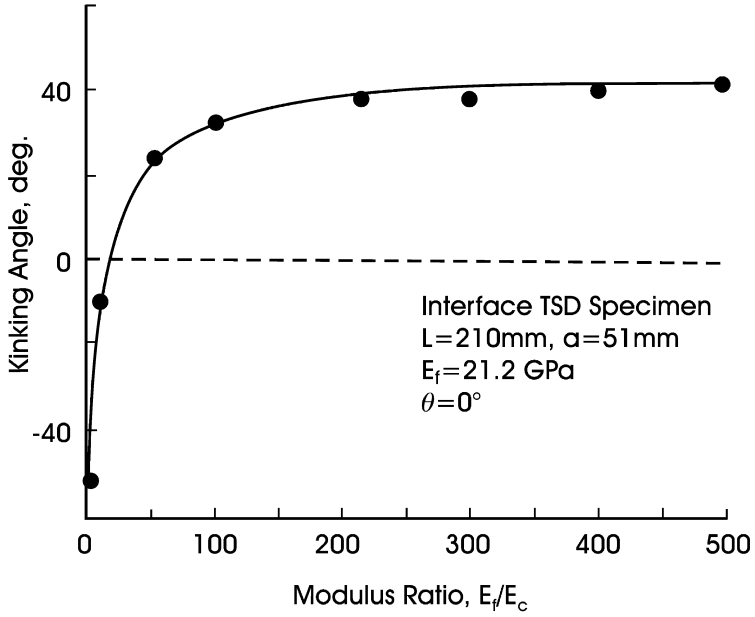

Figure 10.13 Kink angle for interface TSD specimen vs. face-to-core modulus ratio.

It should be pointed out that, in practice, most foam core sandwich panels have large face-to-core modulus ratios $E_f/E_c > 20$, and such panels may be prone to kinking behavior for such loading.

10.5 Cracked Sandwich Beam (CSB) Specimen

One of the earliest proposed debond tests is the cracked sandwich beam (CSB). This test was introduced by Carlsson et al. (1991) in an effort to determine the mode II fracture toughness, G_{IIc}, of the face/core interface. The test is an extension of the mode II end-notched-flexure (ENF) test introduced by Barrett and Foshi (1977) for testing wooden beams, and later applied to composite laminates by Russell and Street (1982). Figure 10.14 illustrates the test principle and the state of stress in an element near the crack tip.

The sign of the interlaminar shear stress, τ_{xz}, is negative ($K_{II} < 0$) and, hence, crack kinking into the core is not an issue. The core element shown in Figure 10.14, however, is loaded in compression and may fail in a crushing mode. Such failure may be avoided by a specific design of the test specimen.

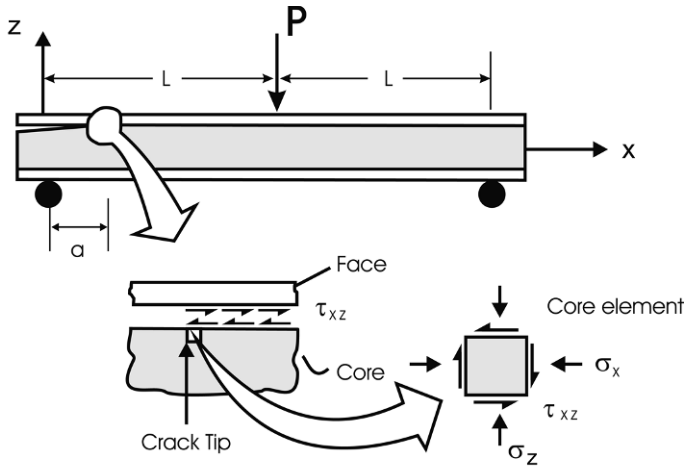

Figure 10.14 The cracked sandwich beam (CSB) test, and state of stress near the crack tip.

The CSB specimen was analyzed by Carlsson et al. (1991) using first-order shear deformation theory, Chapters 3 and 4. The analysis is limited to a symmetric sandwich, but could be extended to sandwich specimens with different face sheets on top and bottom. The presence of a debond will make the specimen more compliant which provides the crack driving force, G. To determine the energy release rate, G, an expression for the CSB compliance as a function of crack length, a, was derived:

$$C = \frac{L^3}{6bD_i} + \frac{L}{2h_c bG_{xz}} + \frac{a^3}{12b}\left[\frac{1}{D_d} - \frac{1}{D_i}\right], \tag{10.21}$$

where L is the half-span length, D_i and D_d are the flexural stiffnesses per unit width of the intact and debonded regions of the specimen, b is the width of the beam, h_c is the core thickness, and G_{xz} is the core shear modulus. The flexural stiffness of the intact region is (Chapter 4)

$$D_i = \frac{E_f h_f}{2}\left(h_c + h_f\right)^2 + \frac{E_f h_f^3}{6} + \frac{E_c h_c^3}{12}, \tag{10.22}$$

where E_f and E_c are the core face and core Young's moduli and h_f is the face thickness. To determine the effective flexural stiffness of the debonded region, D_d, consider the free-body diagram (Figure 10.15). The two regions, 1 and 2, represent the upper and lower faces bonded to the core. The shear forces carried by the upper and lower faces are determined from force equilibrium and compatibility of deformation at the left end.

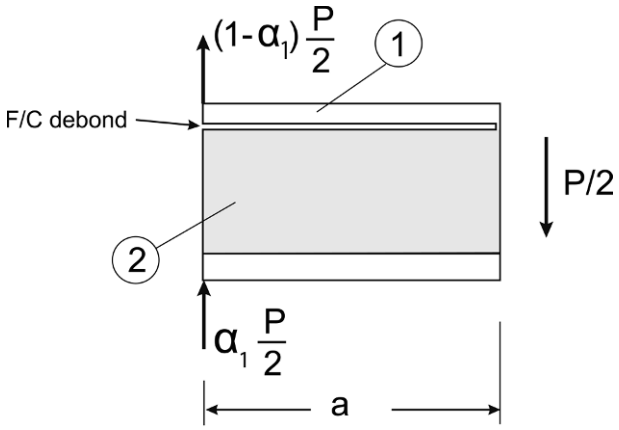

Figure 10.15 Free-body diagram of the debonded region of the CSB specimen.

Analysis of the load partitioning in this region leads to the following expression for the effective flexural stiffness of the debonded region:

$$D_d = (1 - \alpha_1) D_2, \tag{10.23}$$

where α_1 is the load partitioning parameter given by

$$\alpha_1 = \frac{1 + \frac{3D_2}{a^2 h_c G_{xz}}}{1 + \frac{3D_2}{a^2 h_c G_{xz}} + \frac{D_2}{D_1}}, \tag{10.24}$$

in which D represents flexural stiffness per unit width and the subscripts 1 and 2 refer to the upper and lower sub-beams of the debonded region (Figure 10.15)

$$D_1 = \frac{E_f h_f^3}{12}, \tag{10.25a}$$

$$D_2 = D - \frac{B^2}{A}. \tag{10.25b}$$

The A, B, and D terms are the extensional, coupling, and bonding stiffnesses defined in Chapter 9. The energy release rate of the CSB specimen is obtained by differentiation of Equation (10.21) with respect to crack length

$$G = \frac{P^2 a^2}{8b^2} \left[\frac{1}{D_d} - \frac{1}{D_i} \right]. \tag{10.26}$$

The accuracy of the compliance and energy release rate predictions for the CSB specimen have been examined by Quispitupa et al. (2009). The same

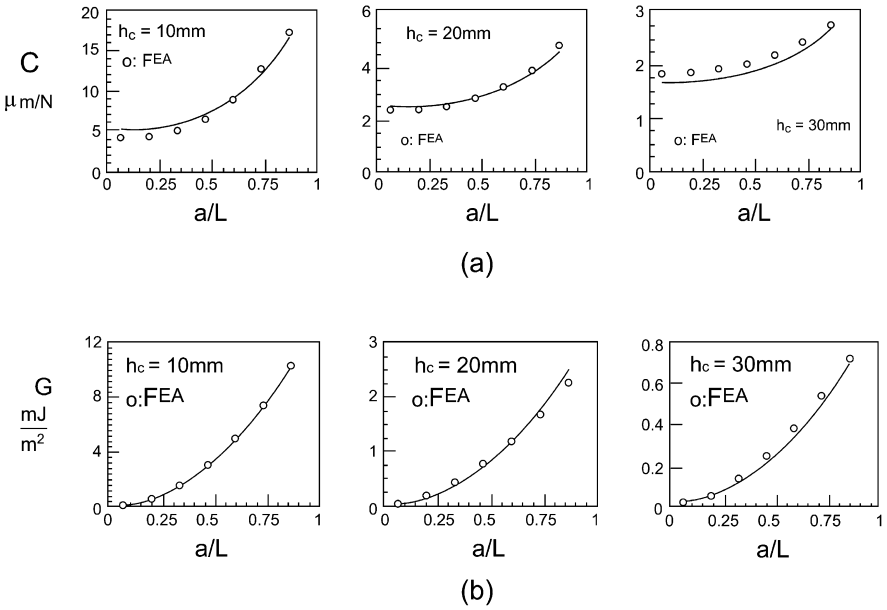

Figure 10.16 Influence of core thickness on the compliance (a) and energy release rate (b) of the CSB specimen. Open circles represent FEA and continuous lines the beam model.

materials and geometries as in the analysis of the DCB specimen (Section 10.3) were used in a detailed finite element analysis of the CSB specimen. Analytical and finite element results for the compliance and energy release rate ($P = 1$ N/mm) are displayed vs. crack length in Figure 10.16. Compliance values determined analytically and numerically are in close agreement, except for short crack lengths (Figure 10.16a). Differences could be attributed to the contact pressure developed between the upper and lower sub-beams in the debonded region. The analytical formulation models load transfer between the lower part of the beam to the upper face sheet through a concentrated force, while the finite element model includes frictionless contact surfaces between the upper and lower sub-beams in order to achieve load transfer for the debonded region. The two contact definitions are not identical and small variations between these two models might be expected.

For the energy release rate, Figure 10.16b shows that the beam theory and finite element results agree closely, lending confidence to the beam theory modeling.

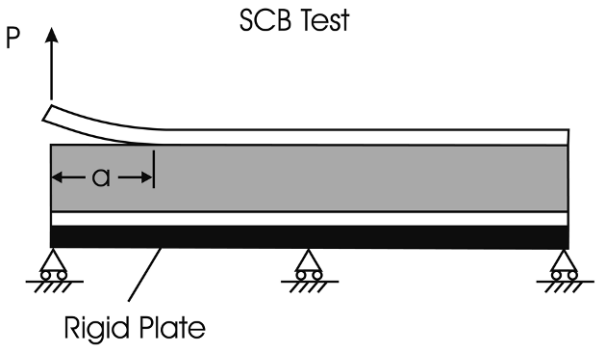

Figure 10.17 Single cantilever beam test configuration.

10.6 Single Cantilever Beam (SCB) Specimen

Cantwell and Davies (1994, 1996), introduced a sandwich debond test method called the "single cantilever beam" (SCB) shown in Figure 10.17.

The bottom surface of the SCB specimen is bonded to a rigid steel plate mounted on a carriage supported by linear roller bearings. Load is applied using a long hinged vertical bar. Since the specimen is attached to the roller-supported base, horizontal forces will not be introduced in the specimen as the upper loaded face deflects. No fracture mechanics of this test has been presented, although the analysis presented for the TSD specimen in Section 10.4 should also be valid for the SCB specimen by setting the tilt angle, $\theta = 0$ in the TSD analysis. Cantwell and Davies (1994, 1996) used this specimen in experimental studies and determined the face/core debond fracture toughness, G_c, from the experimental compliance calibration method. Discussion of the experimental aspects of the test, data reduction, and test results will be presented in Chapter 11.

10.7 Three-Point Sandwich Beam (TPSB) Specimen

Cantwell et al. (1999) proposed a debond test called "three-point bend sandwich beam (TPSB) test", with a support placed under the upper face sheet as shown in Figure 10.18. This arrangement was made possible by removing a section of the core and lower face at the left end of the specimen. This loading arrangement creates a mixed mode I and mode II loading at the crack tip.

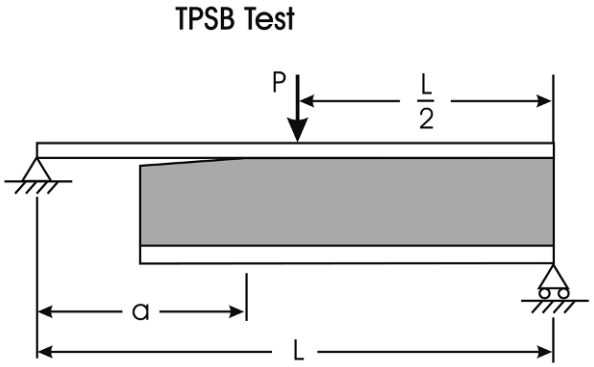

Figure 10.18 Three-point bend sandwich beam (TPSB) test.

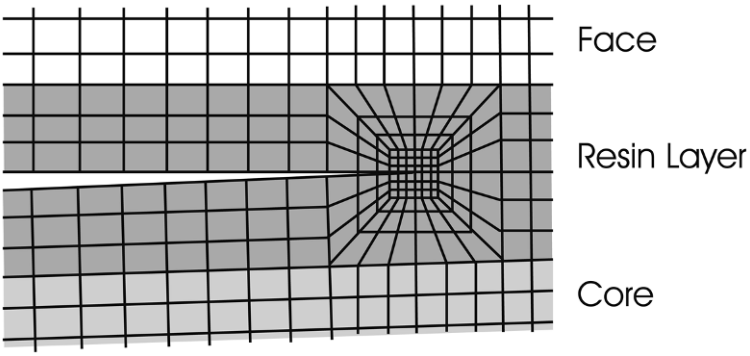

Figure 10.19 Finite element mesh of crack tip region for TPSB specimen.

To determine the strain energy release rate components, G_{I} and G_{II}, and the mode mixity, expressed as $G_{\mathrm{I}}/G_{\mathrm{II}}$, Cantwell et al. (1999) conducted plane strain finite element analysis of the TPSB specimen, with a refined mesh near the crack tip, see Figure 10.19. The crack tip is embedded in a thin resin layer between face and core so as to circumvent complications due to the bimaterial crack tip. A range of crack lengths, a, from 30 to 55 mm was considered. The sandwich beams consisted of 2.5 mm thick glass/polyester faces over a 15 mm thick end-grain balsa core of 175 kg/m^3 density. Cantwell et al. (1990) did not provide the material properties of the face sheets and core, but they should be close to those listed for similar materials in Chapter 1.

The opening and sliding components, G_{I} and G_{II} of the energy release rate, G, were determined by the virtual crack closure technique described in Section 9.1.1. Figure 10.20 shows the mode mixity results presented as the

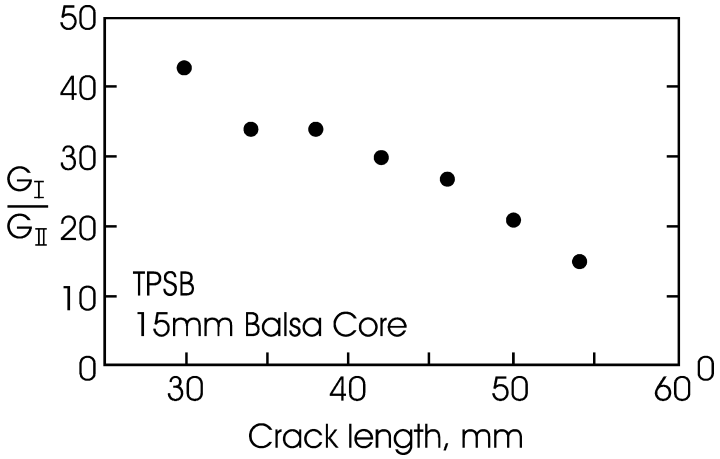

Figure 10.20 Mode ratio G_I/G_{II} for TPSB specimen with balsa core.

ratio G_I/G_{II}, plotted vs. the crack length. It is observed that the mode ratio depends on crack length, although the specimen may be considered as mode I-dominated since G_I is at least a factor of 10 greater than G_{II} over the range of crack lengths considered.

It is observed that the mode mixity is quite a strong function of crack length which is generally a disadvantage, since the fracture resistance typically depends on the mode ratio.

10.8 Mixed Mode Bending (MMB) Specimen

The mixed mode bending (MMB) test was originally developed by Reeder and Crews (1990) for mixed mode delamination fracture characterization of unidirectional composites. This test was recently modified to accommodate sandwich specimens by Quispitupa et al. (2009), see Figure 10.21. The MMB sandwich specimen incorporates a through-width face/core crack at the left edge of the specimen. A vertical, downward load, P, applied to the lever arm, provides an upward directed load at the left end of the debonded face sheet and a downward directed load at the center.

The MMB specimen can be considered as a superposition of the previously discussed CSB and DCB specimens, see Figure 10.22. Analytic expressions for the MMB compliance and energy release rate for symmetric sandwich specimens ($h_{f1} = h_{f2} = h_f$ and $E_{f1} = E_{f2} = E_f$) were derived

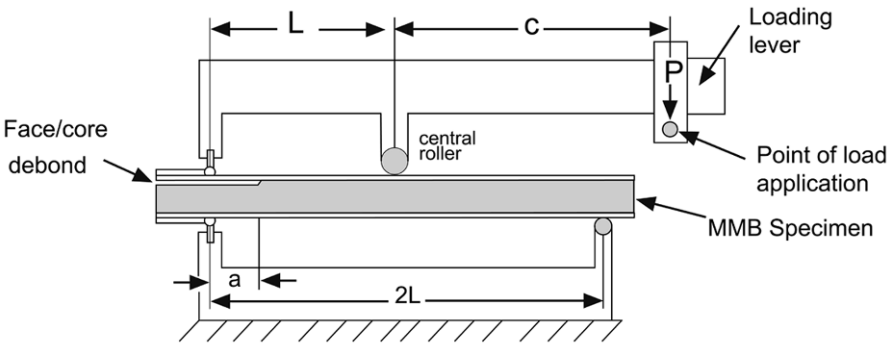

Figure 10.21 MMB test principle and sandwich specimen.

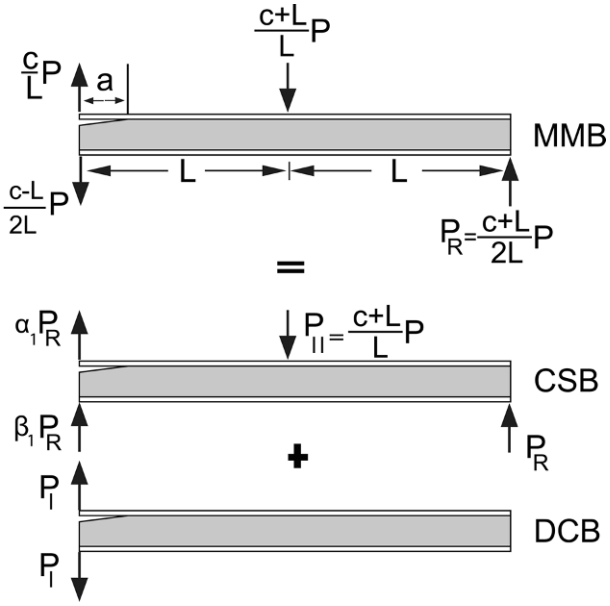

Figure 10.22 Mixed mode loading decomposed into CSB and DCB loadings. α_1 and β_1 are parameters quantifying the load share between the upper and lower parts of the debonded region ($\alpha_1 + \beta_1 = 1$).

based on the load partitioning shown in Figure 10.22 and previous solutions for the CSB and DCB specimens.

The MMB specimen compliance, C, is defined according to

$$C = \frac{\delta_{\text{MMB}}}{P}, \tag{10.27}$$

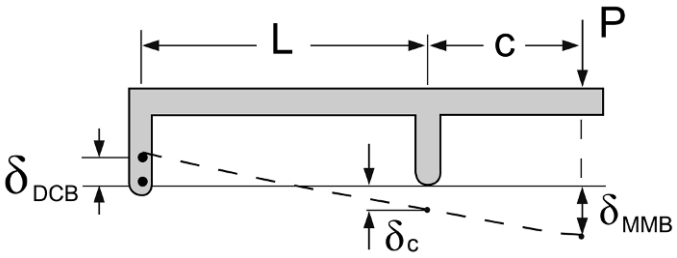

Figure 10.23 Kinematics of MMB specimen deformation.

where δ_{MMB} is the displacement of the load application point calculated from the kinematics of deformation as illustrated in Figure 10.23.

By similar triangles

$$\delta_{\text{MMB}} = \delta_c + \frac{c}{L}\left(\delta_c + \delta_{\text{DCB}}\right). \tag{10.28}$$

where δ_{DCB} refers to the upward displacement of the upper left point of the loading lever and δ_c is the downward displacement of the lever at the center of the beam. The expressions for the MMB compliance and energy release rate are

$$C = \left[\frac{c}{L}C_1 + \frac{c-L}{2L}C_2\right]\left(\frac{c}{L} - \alpha_1\frac{c+L}{2L}\right) + \left(\frac{c+L}{L}\right)^2 C_{\text{CSB}}, \tag{10.29}$$

$$G = \frac{P^2}{2b^2}\left(\begin{array}{l}\frac{c}{L}\left(\frac{c}{L} - \alpha_1\frac{c+L}{2L}\right)\frac{12}{E_f h_f^3}\left[a^2 + 2a\eta^{1/4} + \eta^{1/2}\right] + \\ \frac{c-L}{2L}\left(\frac{c}{L} - \alpha_1\frac{c+L}{2L}\right)\left[\frac{1}{h_c G_{xz}} + \frac{a^2}{\left(D - \frac{B^2}{A}\right)}\right] + \left(\frac{c+L}{L}\right)^2\left(\frac{a^2}{8}\left[\frac{1}{D_d} - \frac{1}{D_i}\right]\right)\end{array}\right), \tag{10.30}$$

where $2L$ is the span length, c is the lever arm distance, a is the crack length, and A, B and D are the extensional, coupling, and bending stiffnesses defined for the DCB specimen in Equations (10.8). η is the elastic foundation modulus parameter defined in Equation (10.7) and D_d and D_i are the flexural stiffness of the debonded and intact region of the beam, defined in Section 10.5. The parameter α_1 is given by Equation (10.24). C_1 and C_2 represent the compliances of the upper and lower legs (1 and 2) of the DCB specimen, Figure 10.4, i.e.

$$C_1 = \frac{\delta_1}{P_1}, \tag{10.31a}$$

$$C_2 = \frac{\delta_2}{P_1} \tag{10.31b}$$

given by

$$C_1 = \frac{4}{E_f h_f^3 b}\left[a^3 + 3a^2\eta^{1/4} + 3a\eta^{1/2} + \frac{3}{2}\eta^{3/4}\right], \tag{10.32a}$$

$$C_2 = \frac{a}{b}\left[\frac{1}{h_c G_{xz}} + \frac{a^2}{3\left(D - \frac{B^2}{A}\right)}\right], \tag{10.32b}$$

where the symbols are defined earlier in this section.

The loads acting on the DCB and CSB specimens (Figure 10.22) are

$$P_I = \frac{c}{L}P - \alpha_1 P_R, \tag{10.33a}$$

$$P_{\text{II}} = \left(1 + \frac{c}{L}\right)P, \tag{10.33b}$$

$$P_R = \frac{c+L}{2L}P. \tag{10.33c}$$

The mode I and II components of the total energy release rate, G (Equation (10.30)) are obtained by substitution of the loads P_{I} and P_{II} into the expressions for G for the DCB and CSB specimens, i.e., $P = P_{\text{I}}$ in Equation (10.6) for the DCB specimen and $P = P_{\text{II}}$ in Equation (10.26) for the CSB specimen. The mode ratio $G_{\text{II}}/G_{\text{I}}$ is

$$\frac{G_{\text{II}}}{G_I} = \left(\frac{P_{\text{II}}a}{2P_I}\right)^2 \frac{\left[\frac{1}{D_d} - \frac{1}{D_i}\right]}{\frac{1}{h_c G_{xz}} + \frac{a^2}{\left(D - \frac{B^2}{A}\right)} + \frac{12}{E_f h_f^3}[a^2 + 2a\eta^{1/4} + \eta^{1/2}]}. \tag{10.34}$$

Notice here that the mode ratio is a global mode ratio. Due to the asymmetric bimaterial character of the sandwich specimen, the local mode mixities expressed in terms of stress intensity factors, will differ (as shown later).

The methodology presented above is not valid when contact between crack faces is present. Contact arises at a lever arm distance, c, when the mode I load (Equation (10.33a)) vanishes. The minimum lever arm distance c, which is required to avoid contact is given by

$$c > \frac{\alpha_1 L}{2 - \alpha_1}. \tag{10.35}$$

For a symmetric specimen, $\alpha_1 = 1/2$, and Equation (10.35) gives $c > L/3$, which is generally used as a limit for MMB testing of monolithic composites. However, for the MMB sandwich specimen, α_1 is very small and therefore the minimum c distance is also very small, which is convenient in order to expand the range crack lengths in the test program.

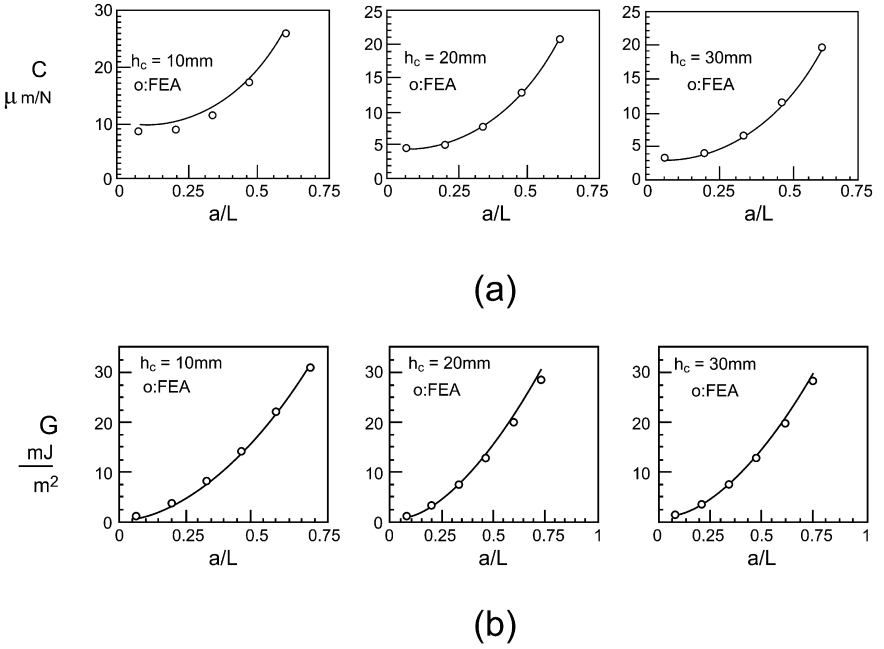

Figure 10.24 Compliance (a) and energy release rate (b) vs. crack length for MMB specimens with core thicknesses of 10, 20 and 30 mm ($c = 25$ mm).

10.8.1 Analytical and Finite Element Results

Quispitupa et al. (2009) conducted extensive parametric finite element analysis of the influence of various geometry and material parameters on the MMB compliance and energy release rate. The energy release rate, G, was extracted from the FEA results using the opening and sliding relative crack flank displacements (Figure 9.4). The same material properties, specimen geometries, and FE mesh, used for the DCB and CSB specimens examined in Sections 10.3 and 10.5, were used for the MMB specimen. The reaction loads from the loading lever were applied at the left cracked end and the center of the MMB specimens, as shown in Figure 10.24.

Figure 10.24 shows MMB compliance and energy release rate for three core thicknesses ($h_c = 10$, 20 and 30 mm) calculated over a range of crack lengths using FEA and the beam analysis (Equations (10.29) and (10.30)) at a fixed lever distance ($c = 25$ mm).

The finite element and beam analysis results are in good agreement. The discrepancies in the compliance for the thinnest specimen ($h_c = 10$ mm)

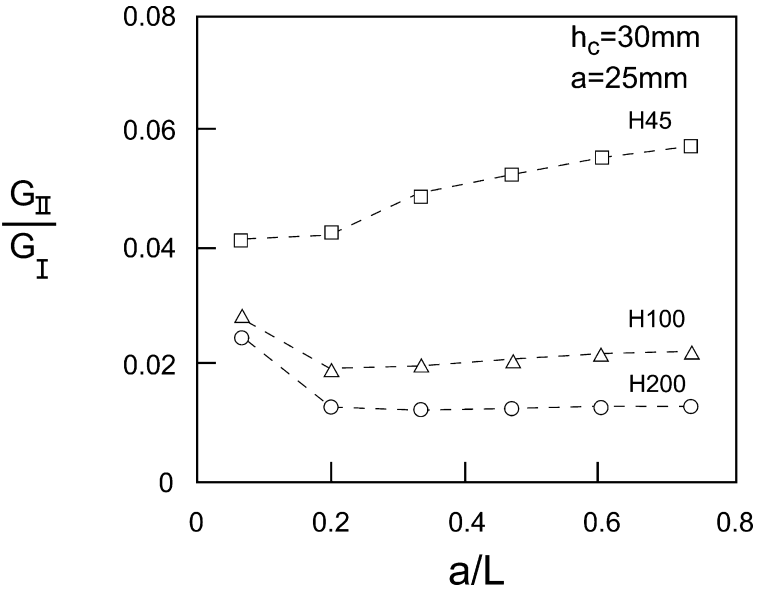

Figure 10.25 Global mode ratio vs. crack length for a set of core materials ($2L = 150$ mm, $b = 35$ mm).

may be due to its small core-to-face thickness ratio ($h_c/h_f = 5$). This thickness ratio is slightly below the "thin face criterion", Equation (1.7). The energy release rate calculated from beam theory and FEA are in very good agreement.

When testing for debond toughness, it is desirable to maintain a constant mode ratio when the crack advances. Hence, the mode ratio $G_{\mathrm{II}}/G_{\mathrm{I}}$ should, ideally, be independent of the crack length. Figure 10.25 shows the global mode mixity ratio, $G_{\mathrm{II}}/G_{\mathrm{I}}$, defined in Equation (10.34) for a sandwich specimen with 2 mm thick glass/polyester face sheets and 30 mm thick H45, H100 and H200 cores at a fixed loading lever distance ($c = 40$ mm) vs. crack length.

The results show that the global mode mixity for the specimens with H100 and H200 cores is approximately constant for $a/L > 0.32$. For the specimens with a H45 core, however, the mode ratio increases with crack length.

As discussed in Chapter 9, a more realistic assessment of the crack loading is obtained by considering the relative crack flank displacements (Figure 9.4). This provides the "local mode mixity" expressed by the phase angle ψ (Equation (10.2)). Sandwich specimens with 2 mm thick glass/polyester face sheets ($E_f = 16.4$ GPa) and a H100 PVC foam core ($E_c = 135$ MPa)

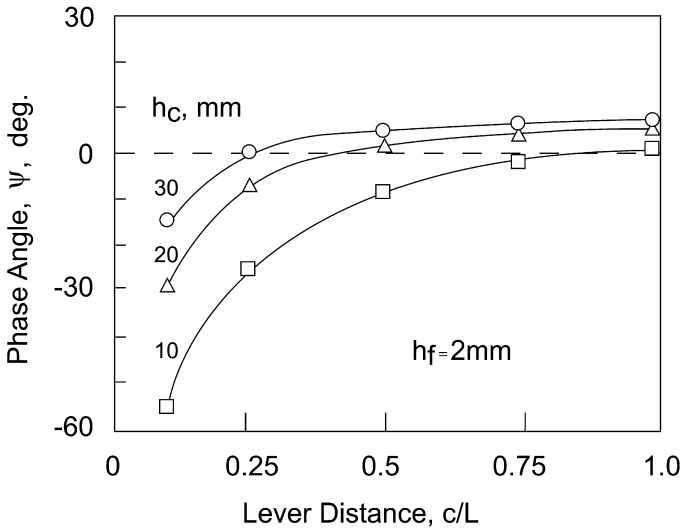

Figure 10.26 Phase angle ψ vs. lever arm distance c/L for a sandwich with $h_f = 2$ mm, $E_f = 16.4$ GPa, and H100 core ($E_c = 135$ MPa) with $h_c = 10$, 20 and 30 mm. $2L = 150$ mm, $b = 35$ mm, and $a = 25$ mm ($a/L = 1/3$).

of 10, 20, and 30 mm were analyzed over a range of lever arm distances ($c/L = 0.1$ to 1). The results are shown in Figure 10.26.

The results show, as expected, that the phase angle increases with increasing lever arm distance (c/L). Furthermore, the results show that increasing core thicknesses (h_c/h_f) leads to increased phase angle. For large lever arm distances, the thickest cores start to display mode I dominance, and crack kinking (Section 9.2) may occur.

10.9 Double Cantilever Beam-Uneven Bending Moments (DCB-UBM) Specimen

The DCB-UBM test principle, shown schematically in Figure 10.27, was introduced by Sorensen et al. (2006) in an effort to measure the debond fracture toughness of composite and sandwich specimens over a large range of mode mixities. The moments M_1, and M_2 are introduced using two arms, adhesively bonded to the cracked end of the DCB specimen. The arms are loaded through a wire/roller arrangement connected to the arms. The assembly is

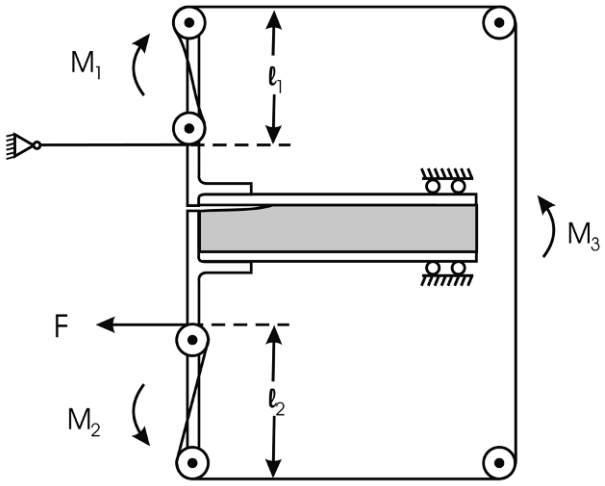

Figure 10.27 Schematic of DCB-UBM test principle for a debonded sandwich specimen.

mounted with the specimen axis oriented vertically in a tall test frame where a moving cross-head provides the pulling force of the wire.

If the wire is flexible and the rollers turn with negligible resistance, the force F in the wire is uniform along the wire and the moments become

$$M_1 = Fl_1, \tag{10.36a}$$

$$M_2 = Fl_2, \tag{10.36b}$$

where the lengths l_1 and l_2 are defined in Figure 10.27 and the signs of M_1 and M_2 are defined positive if both M_1 and M_2 tend to open the crack as shown. A crack loading dominated by mode I is achieved for $M_1/M_2 \approx 1$, i.e. equal opening moments. Mode II-dominated loading is achieved for negative moment ratios M_1/M_2. The magnitudes of the moments may be changed by changing the distances l_1 and l_2. By rearranging the wire as shown in Figure 10.28, the sign of the moment will change.

The uncracked end of the specimen is supported by a roller system (Figure 10.27) that provides rotational constraint by a moment $M_3 = M_1 - M_2$. Further specific details on the test set-up are provided by Sorensen et al. (2007).

The implied loading on the specimen thus consists of the pure moments M_1 and M_2. Following Section 9.4, for this situation we have

$$M_d = M_1; \quad M_s = -M_2; \quad M_b = M_1 - M_2; \quad P_d = P_s = P_b = 0. \tag{10.37}$$

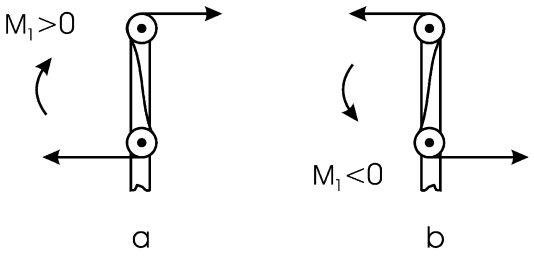

Figure 10.28 Arrangement of the wire to change the sign of the moment a) $M_1 > 0$, b) $M_1 < 0$.

Moreover, from Equation (9.39), the neutral axes of the base part and the substrate are defined by

$$e_b = 0; \quad e_s = \frac{E_f h_f (h_f + h_c)}{2(E_f h_f + E_c h_c)}. \tag{10.38}$$

The load factors on the reduced system are from (9.42b, c) and (9.43b, c)

$$P^* = \frac{E_f h_f}{2D_b}(h_f + h_c)(M_1 - M_2), \quad M_d^* = M_1 - \frac{E_f}{D_b}\frac{h_f^3}{12}(M_1 - M_2), \tag{10.39}$$

and

$$M_s^* = P^* \left(e_s + \frac{h_f + h_c}{2} \right) - M_1, \tag{10.40}$$

where D_b is the rigidity of the base part, given by (9.40b)

$$D_b = \frac{E_f h_f^3}{6} + E_f h_f \frac{(h_f + h_c)^2}{2} + \frac{E_c h_c^3}{12}. \tag{10.41}$$

Then the energy release rate of the debond is obtained from (9.49):

$$G = \frac{1 - \nu_f^2}{2E_f} \left(\frac{P^{*2}}{h_f} + 12 \frac{M_d^{*2}}{h_f^3} \right) + \frac{P^{*2}}{(E_f h_f + E_c h_c)^2} H_1$$
$$+ \frac{P^* M_s^*}{(E_f h_f + E_c h_c) D_s} H_2 + \frac{M_s^{*2}}{D_s^2} H_3, \tag{10.42}$$

where

$$H_1 = \frac{1 - \nu_f^2}{2} E_f h_f + \frac{1 - \nu_c^2}{2} E_c h_c, \tag{10.43}$$

$$H_2 = (1-\nu_c^2)E_c h_c e_s + (1-\nu_f^2)E_f h_f \left(e_s - \frac{h_c}{2} - \frac{h_f}{2}\right), \tag{10.44}$$

$$H_3 = \frac{1-\nu_c^2}{2}E_c h_c \left(\frac{h_c^2}{12} + e_s^2\right) + \frac{1-\nu_f^2}{2}E_f h_f \left[\frac{h_f^2}{3} + \left(\frac{h_c}{2} - e_s\right)\left(\frac{h_c}{2} + h_f - e_s\right)\right], \tag{10.45}$$

and D_s is the rigidity of the substrate part, given by (9.40c)

$$D_s = \frac{E_f h_f^3}{12} + E_f h_f \left(\frac{h_f + h_c}{2} - e_s\right)^2 + \frac{E_c h_c^3}{12} + E_c h_c e_s^2. \tag{10.46}$$